Proceedings World Geothermal Congress 2020+1
Reykjavik, Iceland, April - October 2021

Modelling of Thermally Induced Fracture Slip caused by Fluid Injection During Geothermal Production

Ivar Stefansson, Runar Berge, Inga Berre and Eirik Keilegavlen

ivar.stefansson@uib.no

Keywords: modelling, simulation, reservoir stimulation, fracture slip, hydro-thermo-mechanics

ABSTRACT

In geothermal reservoirs where fluid is injected during stimulation and production, both hydraulic and thermal effects can cause slip of fractures, resulting in permeability changes and induced seismicity. Upon injection, slip may occur as the effective normal traction is reduced through elevated fluid pressure and/or cooling of the host rock. In general, the relative importance of the pressure and thermal effects is assumed to depend on the rate and temperature of the injection. Direct observation in the subsurface being largely unattainable, numerical simulations may provide valuable insights on the processes mentioned above. However, simulation is also highly demanding, due to the coupling of the thermo-hydro-mechanical-chemical (THMC) processes and their interaction with the fractures. For extensively fractured reservoirs, the 3d geometry of the fracture network causes further challenges. In this work, we focus on the thermal component of the normal traction reduction caused by injection of colder fluid during operation of a reservoir with highly permeable fractures. We model a coupled thermo-mechanical problem and its interaction with fluid flow, explicitly accounting for both the matrix and the fractures using a discrete fracture-matrix model. For the mechanical problem, the fractures act as internal boundaries on which a friction law is imposed. Explicitly representing the most prominent fractures facilitates capturing their critical influence on flow. The model allows for dilation and deformation of these fractures due to slip and THM effects. Hence, it also considers the back-coupling effect of changing apertures on fluid flow and deformation. Thermo-hydraulic stimulation of fractured geothermal systems as a consequence of fluid injection during production are studied through transient 3d simulations, utilizing our recently implemented functionality in the open-source simulation toolbox PorePy.

1. INTRODUCTION

Geothermal energy has been identified as an important renewable energy resource with huge untapped production potential. Its usefulness in providing a baseload energy supply makes unlocking this potential highly desirable (IRENA 2017). A key factor limiting the increase of geothermal energy production is the low permeability of potential geothermal reservoirs. This sparked the interest in Enhanced Geothermal Systems (EGS). In such systems, the permeability is enhanced by stimulation of the fractures, which in many cases carry most of the flow. Stimulation can be achieved through various mechanisms, including hydraulically driven and thermally driven ones. The former stimulation type is achieved by elevating the reservoir pressure through fluid injection. This may trigger shearing of pre-existing fractures by reducing the effective normal stress on the fractures, causing an increase in the fracture aperture, and thereby the permeability. If the pressure is sufficiently high, tensile fractures may also form, although this mechanism is believed to be of less importance (McClure 2012).

Thermal stimulation occurs due to contraction of the host rock upon cooling caused by the injected fluid. We distinguish in the following between two such processes. Rapid cooling, which may occur in areas of high flow rates and may be associated with deliberate stimulation of the reservoir, has the potential to trigger the formation of new tensile fractures through high temperature gradients (Ghassemi 2015). Long-term cooling of the reservoir may also lead to rock contraction, relieving the normal stress in a manner similar to the above-mentioned hydraulic shear stimulation. The latter process need not be the result of deliberate stimulation, but may occur during the production phase of energy production (Rawal 2014).

Challenging observation and characterisation are inherent features of deep geothermal systems. These limit both the ability to quantitatively forecast the behaviour in a given reservoir, and the more qualitative understanding of the processes in geothermal systems. Both types of knowledge may be increased through the use of numerical simulations. We shall in this paper focus on the latter type, where the objective is to shed light on individual processes and their interplay by numerical simulations. Specifically, we investigate to which degree long-term cooling during the production phase may contribute to shear events at pre-existing fractures, as reduced normal traction allows for slip on fractures favourably aligned relative to the background stresses.

Inference based on numerical modelling requires a model which precisely captures the dynamics in question. Several model classes exist for dynamics in fractured porous media, with the two classical approaches being the discrete fracture network (DFN) and the equivalent continuum (EC) models. In the former, the fractures are represented explicitly in the model, implying that the geometry of the fracture network may be accounted for directly. All dynamics are assumed to take place in the fractures, and the rock matrix is ignored altogether. In the latter, the fractures are only represented implicitly through upscaled parameters of the rock matrix. The two approaches can be both highly computationally efficient and provide accurate descriptions, especially in processes dominated by the fractures (DFN) or a large number of statistically homogeneous fractures (EC).

Limitations arise for the two classes in processes characterised by the interplay between a limited number of important fractures and the rock matrix. Such processes may be better described by discrete fracture-matrix (DFM) models, where the dominant fractures are modelled explicitly as 2d surfaces embedded in the 3d matrix. The matrix may account for smaller fractures through upscaled parameters, like in EC models. In this work, we apply a DFM model accounting for the flow of fluid and energy both in the matrix and the fractures. We model linear elastic mechanical deformation in the matrix, and enforce non-penetration and a friction relation in the fracture following Hüeber et al. (2008) and Wolmuth (2011). This yields a precise model for the dynamics of the fractures, which also accounts for the dynamics of the matrix.

DFM models are mixed-dimensional, in the sense that the physical processes are modelled and discretised on geometric objects of different dimensions (fractures and matrix). We have implemented this in the open-source simulation toolbox PorePy presented in Keilegavlen et al. (2017), where the matrix and each of the fractures is represented by one object. Discretisation is performed independently on each object, and suitable discrete conditions applied to couple the discretisations together.

2. MODEL

The governing equations follow from mass, energy and momentum conservation statements, whereof the two last are strongly coupled. Mass and energy conservation are imposed in both the matrix and the fractures, and the energy equation includes an advective term to account for energy transported by a fluid. The momentum conservation is imposed in the matrix, whereas we enforce non-penetration and a Coulomb type friction law on the fractures.

We represent the rock matrix of the reservoir by the domain Ω_h with boundary $\partial\Omega_h$, and the fractures by Ω_l. The matrix domain is three-dimensional, while we represent the fractures by two-dimensional objects and associate an aperture a to account for the thickness. Two interfaces, Γ_j^+ and Γ_j^-, are associated with the two sides of the fracture, which also forms an internal boundary $\partial_j\Omega_h$ for Ω_h. Finally, we denote the external boundary by $\partial_i\Omega$, where the subscript i indicates the type of boundary condition.

2.1 Conservation equations

Conservation of momentum reads for the quasi-static case

$$-\nabla\cdot\sigma = \boldsymbol{q}_u \quad \text{in } \Omega_h, \tag{1}$$

with σ denoting the thermo-mechanical stress tensor and $\boldsymbol{q}_u$ the mechanical body forces, in particular the gravity force $\rho\boldsymbol{g}$. Assuming linear thermo-elasticity with a stiffness tensor C, linear thermal expansion coefficient β and bulk modulus K, we obtain

$$\sigma = \frac{C}{2}(\nabla\boldsymbol{u} - \nabla\boldsymbol{u}^T) - 3\beta K(T - T_0).$$

$\boldsymbol{u}$ and T are the unknown displacement and temperature, respectively, while T_0 denotes the initial temperature. The first term on the right-hand side is the linear elasticity relation for small deformations, whereas the second term accounts for stresses due to thermal gradients.

The energy conservation includes a storage term, a term accounting for deformation induced temperature changes, and a thermal flux $\boldsymbol{q}$ consisting of an advective and a diffusive part. We assume constant density ρ, heat capacity c and thermal diffusivity κ, yielding

$$\rho c\frac{\partial T}{\partial t} + 3\beta K T_0\frac{\partial\nabla\cdot\boldsymbol{u}}{\partial t} + \rho c\boldsymbol{v}\cdot\nabla T - \nabla\cdot\kappa\nabla T = q_T \tag{2}$$

On the outer boundary, we pose the following boundary conditions:

$$\begin{aligned}
\boldsymbol{u} &= \boldsymbol{g_u} && \text{on } \partial_{\boldsymbol{u}}\Omega\\
\sigma\cdot\boldsymbol{n} &= \boldsymbol{g}_\sigma && \text{on } \partial_\sigma\Omega\\
T &= g_T && \text{on } \partial_T\Omega\\
\boldsymbol{q}\cdot\boldsymbol{n} &= g_{\boldsymbol{q}} && \text{on } \partial_{\boldsymbol{q}}\Omega.
\end{aligned}$$

Assuming that the fluid flux $\boldsymbol{v}$ does not depend on thermo-mechanical system comprised of Equations (1) and (2), it will be computed independently according to conservation of fluid mass. Inserting Darcy's law for the flux, neglecting gravity effects and assuming the fluid to be incompressible, we arrive at an equation in terms of the unknown fluid pressure p,

$$\nabla\cdot\boldsymbol{v} = -\nabla\cdot\frac{K}{\mu}\nabla p = q_p \tag{3}$$

with K, μ and q_p denoting permeability, viscosity and fluid sources, respectively. The balance equation is complemented by the boundary conditions

$$\begin{aligned}
p &= g_p && \text{on } \partial_p\Omega\\
\boldsymbol{v}\cdot\boldsymbol{n} &= g_v && \text{on } \partial_{\boldsymbol{v}}\Omega.
\end{aligned}$$

We impose Equations (2) and (3) in both Ω_h and Ω_l. To couple the equations, we consider the fluxes across $\partial_j\Omega_h$ with outwards pointing normal vector $\boldsymbol{n}$. The fluxes will appear as a boundary condition for Ω_h, and as a source/sink term for Ω_l. For the mass balance, we impose a Darcy type constitutive law, so that the flux from Ω_h to Ω_l satisfies

$$\boldsymbol{v}_j\cdot\boldsymbol{n} = -\frac{\mathrm{K}_n/\mu}{a/2}(p_l - tr\ p_h).$$

Here, K_n, p_l and $tr\ p_h$ are the permeability of the fracture in the normal direction, the pressure of the fracture and the trace of the pressure on the boundary of the matrix, respectively. For the energy balance, the diffusive term is handled in direct analogy to that of the mass balance, with the normal thermal diffusivity κ_n replacing K_n. For the advective term, we apply a first order upwind scheme for the temperature gradient, obtaining

$$(\boldsymbol{v}\cdot\nabla T)_j = \begin{cases} \boldsymbol{v}_j\cdot\boldsymbol{n}\; tr\, T_h & \text{if } \boldsymbol{v}_j\cdot\boldsymbol{n} > 0 \\ \boldsymbol{v}_j\cdot\boldsymbol{n}\; T_l & \text{if } \boldsymbol{v}_j\cdot\boldsymbol{n} < 0. \end{cases}$$

For a thorough description and derivation of these coupling conditions, we refer to Berre et al. (2018).

Note that we have assumed local thermal equilibrium, enabling us to use a single unknown temperature and effective parameters (ρ, c, κ, β). Similarly, we use an effective stiffness tensor C accounting for the presence of pore fluid in the rock matrix.

2.2 Fracture deformation

The nonpenetration condition and friction law at the fracture relate the fracture displacement to the contact traction, i.e. the traction caused by the contact between the two fracture surfaces. Denoting the displacement on the interfaces on either side of a fracture as $\boldsymbol{u}^+$ and $\boldsymbol{u}^-$, we define the displacement jump over a fracture as

$$[\boldsymbol{u}] = \boldsymbol{u}^+ - \boldsymbol{u}^-.$$

Denoting the outwards pointing normal vector on the positive side by $\boldsymbol{n}^+$, we define the contact traction of the fracture to equal the trace of the thermo-elastic traction on the positive side

$$\boldsymbol{T}_l = tr\, \boldsymbol{T}_h^+ = tr(\sigma^+\cdot\boldsymbol{n}^+).$$

We further decompose the traction and the displacement jump in their normal and tangential components as follows

$$\begin{aligned} [u]_n &= [\boldsymbol{u}]\cdot\boldsymbol{n}^+, & [\boldsymbol{u}]_\tau &= [\boldsymbol{u}] - [u]_n\boldsymbol{n}^+, \\ T_n &= \boldsymbol{T}_l\cdot\boldsymbol{n}^+, & \boldsymbol{T}_\tau &= \boldsymbol{T}_l - T_n\boldsymbol{n}^+. \end{aligned}$$

Note that with our choice of normal vector, negative $[\boldsymbol{u}]_n$ corresponds to an opening of the fracture. Similarly, negative T_n indicates a compressive force acting on the fracture wall (away from the fracture).

The nonpenetration condition ensures that (i) the normal component of the displacement jump is nonpositive, (ii) either the normal contact traction is zero or the two sides of the fractures are in contact and (iii) the normal component of the contact traction is nonpositive:

$$\begin{aligned} [u]_n &\le 0, \\ T_n[u]_n &= 0, \\ T_n &\le 0. \end{aligned}$$

If the fracture is open, i.e. the displacement jump is negative, the contact forces must be zero on both sides of the fracture. Otherwise, we enforce Newton's third law:

$$\boldsymbol{T}^+ = -\boldsymbol{T}^-.$$

Finally, the Coulomb friction model relates the traction and displacement jump in the tangential direction by the friction coefficient F

$$\begin{aligned} &\|\boldsymbol{T}_\tau\| \le -FT_n \\ &\|\boldsymbol{T}_\tau\| < -FT_n \quad \rightarrow \quad [\dot{\boldsymbol{u}}]_\tau = 0 \\ &\|\boldsymbol{T}_\tau\| = -FT_n \quad \rightarrow \quad \exists\alpha\in\mathbb{R}:\ \boldsymbol{T}_\tau = -\alpha^2[\dot{\boldsymbol{u}}]_\tau, \end{aligned} \tag{4}$$

with $\dot{\boldsymbol{u}}$ being the displacement velocity and $\|\cdot\|$ the L^2 norm. The conditions state (i) the friction bound, (ii) that there is no slip if the bound is not reached and (iii) that, when the bound is reached, the tangential sliding velocity is parallel to and in the opposite direction of the tangential traction. For further details on the contact mechanics model, we refer to Berge (2019).

2.3 Discretisation

The spatial and temporal discretisation of the conservation equations is achieved using Finite Volume (FV) schemes and Implicit Euler, respectively. The spatial grids consist of tetrahedra and triangles for the matrix and fractures, respectively, and are constructed such that the triangles coincide with faces of the matrix tetrahedra.

For the coupled TM equations, we apply a scheme introduced by Nordbotten (2016) for the Biot equations, i.e. a coupled hydro-mechanical (HM) system. The scheme is termed the MPSA/MPFA-FV and provides accurate representation of coupled flow and mechanics; particularly local conservation of mass and momentum. In this work, we exploit the similarity of the TM and HM equations to apply the scheme to the former. The additional advective term is discretised using a first order upwind scheme, i.e. the temperature flux between cells K^i and K^j sharing a face π is

$$(\boldsymbol{v}\cdot\nabla T)_\pi = \begin{cases} \boldsymbol{v}_\pi\cdot\boldsymbol{n}_{i,\pi}T^i & \text{if } \boldsymbol{v}_\pi\cdot\boldsymbol{n}_{i,\pi} > 0 \\ \boldsymbol{v}_\pi\cdot\boldsymbol{n}_{i,\pi}T^j & \text{if } \boldsymbol{v}_\pi\cdot\boldsymbol{n}_{i,\pi} < 0, \end{cases}$$

with $\boldsymbol{n}_{i,\pi}$ denoting the outward normal vector of K^i at the face π.

For the mass balance, we use the Multi-Point Flux Approximation (MPFA) scheme described by Aavatsmark (2002). This is the same discretisation as we use for the diffusive term of the energy balance.

The contact conditions are discretised using a mortar variable $\boldsymbol{u}_j$ representing the displacement on the two sides of the fracture and corresponding to $\boldsymbol{u}^+$ and $\boldsymbol{u}^-$, and a variable for the fracture surface traction $\boldsymbol{T}_l$. The variable $\boldsymbol{u}_j$ is related to the higher-dimensional displacements by setting a Dirichlet condition on $\delta_j \Omega_i$.

The force balance at the fracture is discretised by projecting the higher-dimensional contact tractions from $\delta_j \Omega_h$ to Γ_j and the fracture traction $\boldsymbol{T}_l$ from Ω_l to Γ_j and enforcing

$$\boldsymbol{T}_l = tr\, \boldsymbol{T}_h^+ \quad \text{and} \quad \boldsymbol{T}_l = -tr\, \boldsymbol{T}_h^-.$$

The Coulomb friction model is discretised by projecting $[\boldsymbol{u}_j]$ onto Ω_l and relating it to $\boldsymbol{T}_l$ according to Eq. (4). The nonlinearity caused by the need to differentiate between open, sticking and slipping regions of the fracture is handled by a semi-smooth Newton method, see Hüeber (2008) and Berge (2019).

3. NUMERICAL SIMULATION

The simulation is designed to resemble a geothermal reservoir in the production and re-injection phase, with some idealisations (such as the fracture geometry) allowing us to focus on understanding the physical mechanisms. In particular, we investigate long-term cooling of a reservoir and the effect on fracture reactivation. In light of the idealisations, we stress that the results should be interpreted in a qualitative way; for simulations to have any potential of quantitative prediction, more precise, site specific geometries and parameters are required.

We consider a cubic domain with edge length 1.2 km centred 1.0 km below the surface and containing three fractures. Injection of cold fluid takes place in one grid cell in one fracture and production in a cell in another fracture as indicated in Figure 1, whereas no wells are included in the last fracture or the rock matrix. Assuming the domain to be large in comparison to the region in which the studied dynamics take place, we assign stress boundary conditions imitating anisotropic background stresses, and Dirichlet boundary conditions for both temperature and pressure. Before injection sets in and the transient simulation, the domain is allowed to equilibrate under the background stresses. Under these conditions, no slip occurs, as may be seen from the first time step shown in Figure 2.

The full set of parameters is listed in Table 1. The parameters are chosen to resemble those of granite and water at typical reservoir conditions. Constant values are used for all parameters; those sensitive to temperature are evaluated at the initial reservoir temperature. The matrix porosity is assumed to be small enough that the rock properties can be used for Ω_h, whereas the fracture is assumed to be filled with fluid and obey a cubic law for the permeability.

Table 1: Material properties (left) and boundary and initial conditions and sources (right).

Rock	
Density, ρ	$2.7 \cdot 10^3$ kg/m^3
Specific heat capacity, c	$7.9 \cdot 10^2$ J/kg K
Thermal conductivity, κ	3.1 W/kg K
Thermal expansion, β	$1.6 \cdot 10^{-5}$ m/m K
Matrix permeability, K	10^{-16} m^2
Bulk modulus, K	$2{,}2 \cdot 10^{10}$ Pa
Poisson's ratio, ν	0.2
Fluid	
Density, ρ	$1.0 \cdot 10^3$ kg/m^3
Specific heat capacity, c	$4.0 \cdot 10^3$ J/kg
Thermal conductivity, κ	$6.0 \cdot 10^{-1}$ W/kg K
Thermal expansion, β	$6.5 \cdot 10^{-4}$ m/m K
Bulk modulus, K	$2.5 \cdot 10^9$ Pa
Viscosity, μ	$1.8 \cdot 10^{-4}$ Pa s

Maximum horizontal stress, σ_H	$-3/2\,\rho_r g z$ Pa
Minimum horizontal stress, σ_h	$-7/8\,\rho_r g z$ Pa
Vertical stress, σ_v	$-\rho_r g z$ Pa
Boundary and initial temperature	150 ℃
Boundary pressure, p_D	$5.0 \cdot 10^7$ Pa
Source flow rate	$1.5 \cdot 10^{-3}$ m^3/s
Injection source temperature	50 ℃
Simulation time	6 years
Number of time steps	30
Hydraulic aperture, a	$1 \cdot 10^{-3}$ m
Friction coefficient, F	0.5

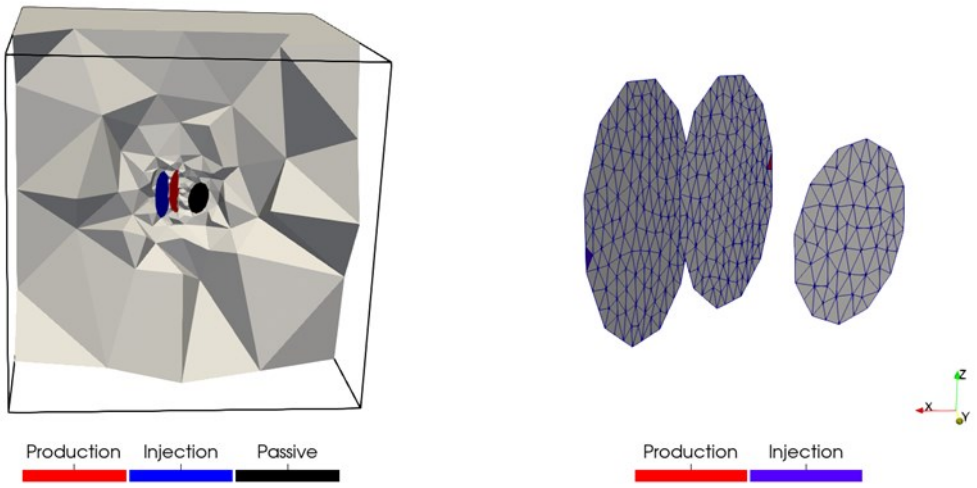

Figure 1: Geometry of the fracture network and spatial grids. The three fractures are marked according to what type of well is located on them to the left, and the locations of the two wells are indicated in the close-up to the right.

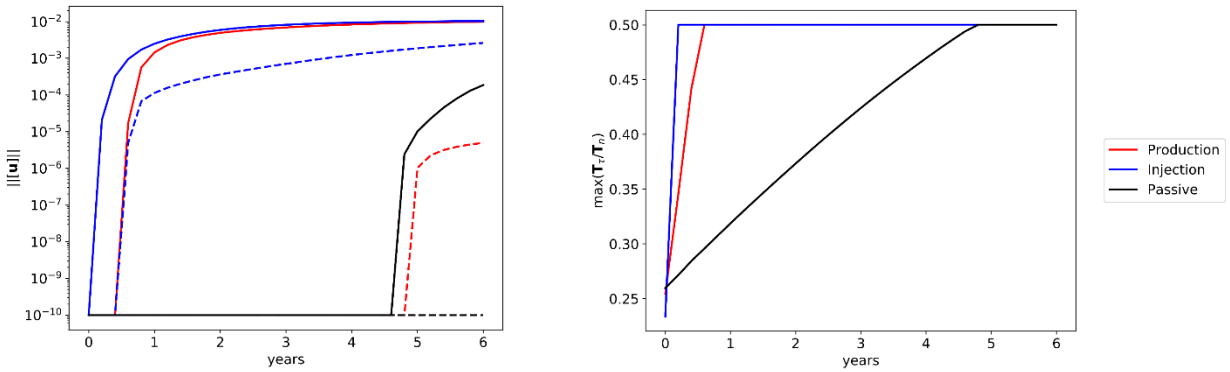

Figure 2: Norm of the displacement jump (left) and maximum traction ratio (right) for each fracture plotted against time. The normal and tangential parts of the displacement jump are shown in dashed and solid lines, respectively. Traction ratios are only shown for the parts of the fractures which are in contact.

The temperature plots shown to the left in Figure 3 show a significant decrease of temperature first in the injection fracture, then also in the production fracture at the latter stages of the simulation.

As indicated in Figure 2, the injection leads to a decrease of the normal traction on all three fractures. The effect manifests first on the injection fracture, then on the production fracture and finally on the passive fracture, which is furthest away from the injection point. When the traction ratio $\|\boldsymbol{T}_\tau\|/T_n$ reaches the friction bound of 0.5, tangential displacement jumps appear. We note that when the passive fracture slips, the temperature in and around that fracture is still very close to the initial temperature, as shown in the bottom left corner of Figure 3. Thus, the relieved normal traction results from the thermal contraction at some distance away from the fracture in question.

Normal displacements only appear on the injection and production fracture, where there is most cooling. The injection fracture opens almost immediately, whereas the production fracture opens towards the end of the simulation, long after it starts to slip tangentially. At the passive fracture, the temperature reduction is insufficient to overcome the normal traction from the background stresses.

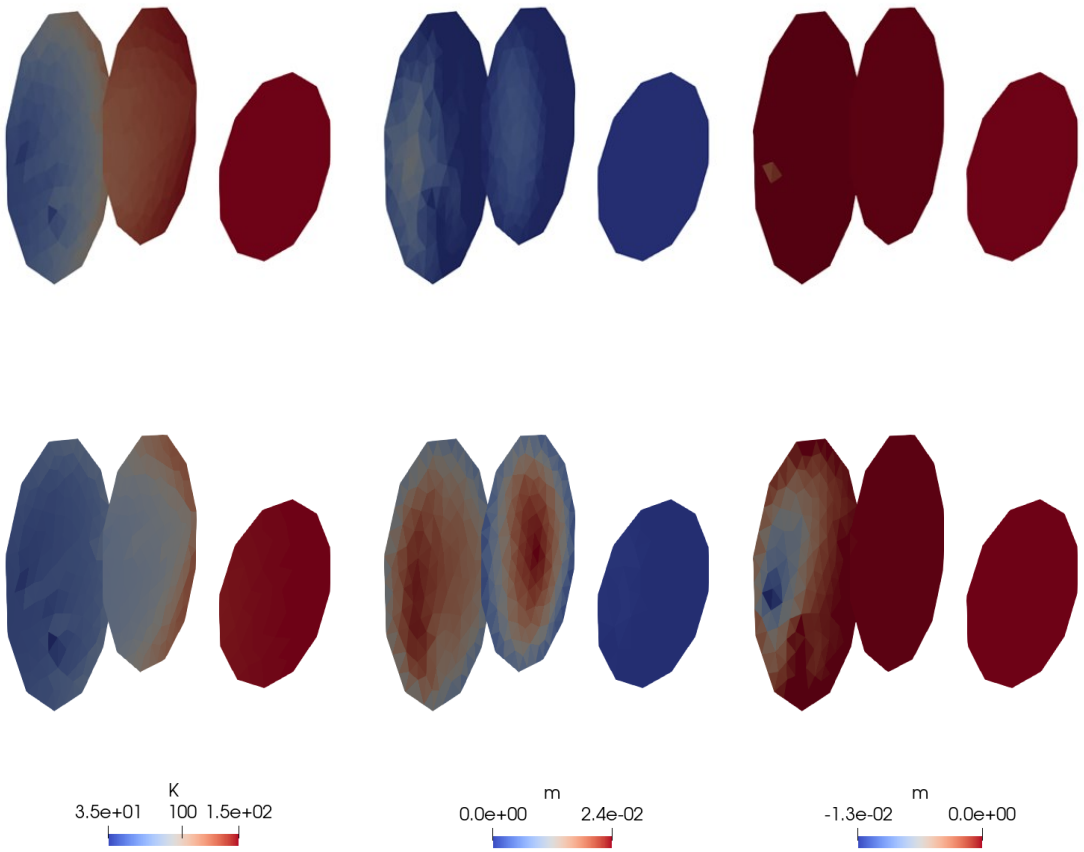

Figure 3: From left to right: Temperature distribution, tangential displacement jumps (magnitude) and normal displacement jumps for all three fractures, all shown after one (top) and six (bottom) years. Note that according to the chosen sign convention, negative normal displacement jumps correspond to fracture opening.

4. CONCLUSION

The simulations presented demonstrate how long-term thermal cooling of a geothermal reservoir may lead to both fracture reactivation with corresponding slip events and normal opening of fractures. We note especially the non-local nature of the process: Fractures are reactivated also outside the cooled region through normal stress relief mechanisms.

The results were obtained using a sophisticated DFM model for coupled thermo-mechanical processes, accounting for fluid flow and energy transport in both fractures and rock matrix, as well as deformation of the matrix and a contact law at the fractures. The detail of the model allows us to accurately study the interplay between the coupled physical processes and the effect on individual, explicitly modelled fractures.

REFERENCES

Aavatsmark, I.: An Introduction to Multipoint Flux Approximations for Quadrilateral Grids, *Computational Geosciences,* **6**, (2002), 405–432.

Berge, R.L., Berre, I., Keilegavlen, E., Nordbotten J.M., and Wohlmuth, B.: Finite volume discretization for poroelastic media with fractures modeled by contact mechanics, arXiv:1904.11916 [math.NA], (2019).

Berre, I., Boon, W.M., Flemisch, B., Fumagalli, A., Gläser, D., Keilegavlen, E., Scotti A., Stefansson I., Tatomir, A.: Call for participation: Verification benchmarks for single-phase flow in three-dimensional fractured porous media, arXiv:1809.06926 [math.NA], (2018).

Ghassemi, A., Tarasovs, S.: Analysis of Fracture Propagation under Thermal Stress in Geothermal Reservoirs, *Proceedings World Geothermal Congress 2015,* (2015).

Huëber, S.: Discretization techniques and efficient algorithms for contact problems, PhD thesis, Universität Stuttgart, http://dx.doi.org/10.18419/opus-4837, (2008).

Huëber, S., Stadler, G., Wohlmuth, B.: A primal–dual active set algorithm for three-dimensional contact problems with Coulomb friction, *SIAM J. Sci. Comput*. 30, 572–596, (2008).

IRENA: Geothermal Power: Technology Brief, *International Renewable Energy Agency*, Abu Dhabi, (2017).

Jansen, G., and Miller, S.A.: On the Role of Thermal Stresses during Hydraulic Stimulation of Geothermal Reservoirs, *Geofluids,* (2017).

Keilegavlen, E., Fumagalli, A., Berge, R., Stefansson, I., Berre, I: PorePy: An Open-Source Simulation Tool for Flow and Transport in Deformable Fractured Rocks, arXiv:1712.00460 [cs.CE], (2017).

McClure, W. M.: Modeling and characterization of hydraulic stimulation and induced seismicity in geothermal and shale gas reservoirs. PhD diss., Stanford University (2012).

Nordbotten, J.: Stable cell-centered finite volume discretization for biot equations, *SIAM Journal on Numerical Analysis*, **54** (2), 942-968, (2016). doi:10.1137/15M1014280.

Rawal, C., Ghassemi, A.: A reactive thermo-poroelastic analysis of water injection into an enhanced geothermal reservoir, *Geothermics,* **50**, (2014).

Wolmuth, B.: Variationally consistent discretization schemes and numerical algorithms for contact problems, *Acta Numerica,* Cambridge University Press, **20**, (2011), pp. 569–73, doi: 10.1017/S0962492911000079.